Ciência & Engenharia (Science & Engineering Journal) ISSN 1983-4071
23 (1): 37 – 45, jan. – jun. 2014

MODELING OF A WIND ENERGY CONVERSION SYSTEM FOR DYNAMIC ANALYSIS USING ALTERNATIVE TRANSIENTS PROGRAM

MODELAGEM DE UM SISTEMA DE CONVERSÃO DE ENERGIA EÓLICA PARA ANÁLISE DINÂMICA USANDO O ALTERNATIVE TRANSIENTS PROGRAM

Daniel Araújo Caixeta[1], Geraldo Caixeta Guimarães[2], Marcelo Lynce Ribeiro Chaves[3]
Universidade Federal de Uberlândia, Faculdade de Engenharia Elétrica, Uberlândia, MG, Brasil, CEP: 38400-902,
Tel.: +55 (34) 3239-4727
[1]E-mail: daniel_engeletrica@yahoo.com.br
[2]E-mail: gcaixeta@ufu.br
[3]E-mail: lynce@ufu.br

ABSTRACT

In recent decades, wind energy has gained great prominence in various parts of the world. This fact shows the need to develop advanced studies in order to evaluate the dynamic behavior of modern wind turbines. Within this context, this work presents a mathematical and computer modeling in ABC reference frame of a Wind Energy Conversion System (WECS) using a Permanent Magnet Synchronous Generator (PMSG). The functionality of the constructed model is verified through computer simulations of wind turbulences and load changes using the free software Alternative Transients Program (ATP), especially with its "MODELS" interface.

Keywords: Alternative Transients Program, Load changes, Permanent Magnet Synchronous Generator, Wind Energy Conversion System, Wind turbulences.

RESUMO

Nas últimas décadas a energia eólica tem ganhado grande notoriedade em várias partes do mundo. Este fato mostra a necessidade de se desenvolver estudos avançados a fim de avaliar o comportamento dinâmico de turbinas eólicas modernas. Dentro deste contexto, este trabalho apresenta uma modelagem matemática e computacional no sistema ABC de um Sistema de Conversão de Energia Eólica dotado de um Gerador Síncrono de Imã Permanente. A funcionalidade do modelo construído é verificado através de simulações computacionais de turbulências no vento e variações de carga utilizando o *software Alternative Transients Program* (ATP), especialmente por meio de sua interface "MODELS".

Palavras-chave: Programa de transientes alternativos, Variações de carga, Gerador Síncrono de Imã Permanente, Sistema de Conversão de Energia Eólica, Turbulências eólicas.

1 – INTRODUCTION

Wind energy is a green and renewable energy source with low operation cost and it has played an important role in power grid expansion in several countries, totaling 283 GW of worldwide installed capacity in 2012, which is 45 GW larger than in 2011 (BRAY *et al*., 2013).

Talking about modern wind systems, Permanent Magnet Synchronous Generators (PMSG) have been frequently used in variable speed wind turbines (BARAZARTE *et al*., 2011; ALEPUZ *et al*., 2013) mainly because a gearbox installation is not required, thereby reducing weight, cost and maintenance (FREIRE *et al*., 2014), providing higher reliability and decreasing noise emissions during low speed operation (LÓPEZ-ORTIZ *et al*., 2012).

Additionally, when a PMSG is connected to a frequency conversion electronic system, voltage regulator and turbine governor are eliminated, enabling the adjustment of active and reactive power injected into power grid and the maintenance of voltage and frequency levels within appropriate ranges (LI *et al*., 2008).

This scenery has led to the development of many researches about the dynamic behavior of PMSG-based wind turbines, where its mathematical modeling has been chiefly carried out in the DQ0 reference frame. Computer simulations are normally performed using MatLab (BYSTRYK and SULLIVANN, 2011; ALEPUZ *et al*., 2013) and including wind variations. Eventually, other associated computer programs are adopted to represent the wind and turbine mechanical parts (SHARIATPANAH *et al*., 2013).

Alternative Transients Program (ATP), a free distribution version of its precursor Electromagnetics Transients Program (EMTP), has gained a great prominence in commercial, academic and scientific scope around the world. This computer platform provides time domain techniques functions, mainly through its ATPDraw and MODELS interfaces, which are appropriate features for modeling the whole Wind Energy Conversion System (WECS). Besides, ATP offers excellent graphics capabilities and a friendly interaction with the user. Thereby, these attributes have motivated the utilization of ATP for computer simulations presented in this work.

This paper presents a mathematical and computer modeling of a WECS with a PMSG-based wind turbine supplying an isolated load. The ABC reference frame is used instead of DQ0 system especially because real generator parameters are better employed in such representation. The functionality of the implemented

modeling is verified through computer studies performed with ATP taking into account normal and abnormal wind speed conditions, besides sudden load changes.

2 – MATHEMATICAL MODELING

In Figure 1 is presented the electromechanical topology of WECS focused in this work.

Figure 1 – Electromechanical topology of WECS

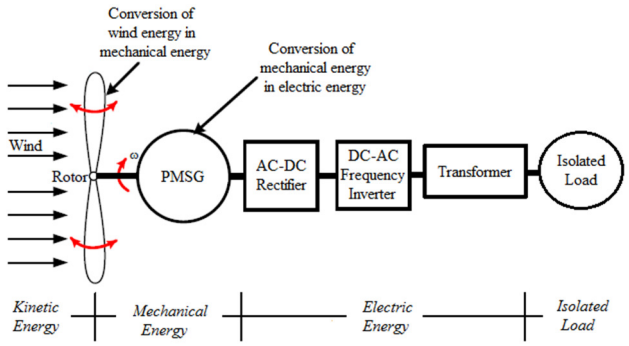

2.1 Wind Modeling

The mathematical formulation v_{wind} chosen for representing the wind speed in this work is a four-component model defined by Equation (1), as described in Anderson and Bose (1983). This expression is attractive since it expresses both the natural intensity of primary energy source as well as the possible occurrence of wind turbulences, including its random component.

$$v_{wind} = v_{base} + v_{gust} + v_{ramp} + v_{noise} \tag{1}$$

Where:

v_{base}: base wind speed component (m/s);
v_{gust}: gust wind speed component (m/s);
vramp: ramp wind speed component (m/s);
vnoise: noise wind speed component (m/s).

The base wind speed component or average wind velocity is always present when the turbine is in operation and it is represented by Equation (2), where K_B is a constant term.

$$v_{base} = K_B \tag{2}$$

The gust wind speed component is described by Equations (3) and (4):

$$v_{gust} = \begin{cases} 0 & t < t_{s\_gust} \\ v_{\cos} & t_{s\_gust} < t < \left(t_{s\_gust} + T_{gust}\right) \\ 0 & t > \left(t_{s\_gust} + T_{gust}\right) \end{cases} \tag{3}$$

$$v_{\cos} = \left(\frac{AMP_{gust}}{2}\right)\left\{1 - \cos 2\pi\left[\left(\frac{t}{t_{s\_gust}}\right) - \left(\frac{t_{s\_gust}}{T_{gust}}\right)\right]\right\} \tag{4}$$

Where:

t: time;
Tgust: gust period (s);
ts_gust: gust starting time (s);
AMPgust: gust peak (m/s).

The ramp wind speed component is described by Equations (5) and (6):

$$v_{ramp} = \begin{cases} 0 & t < t_{i\_ramp} \\ v_r & t_{i\_ramp} < t < t_{f\_ramp} \\ 0 & t > t_{f\_ramp} \end{cases} \tag{5}$$

$$v_r = AMP_{ramp}\left[1 - \frac{\left(t - t_{e\_ramp}\right)}{\left(t_{s\_ramp} - t_{e\_ramp}\right)}\right] \tag{6}$$

Where:

t_{s_ramp}: ramp starting time (s);
t_{e_ramp}: ramp ending time (s);
AMP_{ramp}: ramp peak (m/s).

The last wind velocity component is the random noise term, which incorporates the wind randomness, defined by Equations (7) and (8). As well as the base speed value of the wind, this component is always present because of small wind turbulences.

$$v_{noise} = 2\sum_{i=1}^{N}\left[S_V\left(\omega_i\right)\Delta\omega\right]^{\frac{1}{2}}\cos\left(\omega_i t + \phi_i\right) \tag{7}$$

$$\omega_i = \left(i - \frac{1}{2}\right)\Delta\omega \tag{8}$$

Where:

ϕ_i: random variable with uniform probability density in the interval from 0 to 2π;
Δω: angular velocity variation (rad/s);
N: total number of terms.
Note: N = 50 and Δω = 0.5 – 2.0 rad/s provide results of excellent accuracy (ANDERSON and BOSE, 1983).

The function $S_v(\omega_i)$ is the spectral density function defined by Equation (9):

$$S_V\left(\omega_i\right) = \frac{2K_N F^2\left|\omega_i\right|}{\pi^2\left[1 + \left(F\omega_i/\mu\pi\right)^2\right]^{\frac{4}{3}}} \tag{9}$$

Where:

K_N: surface drag coefficient;
F: turbulence scale;
μ: mean wind speed at reference height [m/s].
Note: K_N = 0.004 and F = 2000 provide results of excellent accuracy (ANDERSON and BOSE, 1983).

As ATPDraw libraries do not provide the adopted wind model, it was necessary to develop it using the MODELS interface that uses a structured programming language similar to FORTRAN. This alternative allowed

the production of a new block component representing the wind and its variations, as shown in Figure 2.

Figure 2 – Wind block

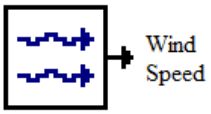

The wind block constructed has no input nodes, and the wind speed is determined by its components v_{base}, v_{gust}, v_{ramp} and v_{noise}, and made available at its output node.

It is important to mention that the input data are entered or modified by double clicking on the icon. The same procedure is valid for the others icons of this work.

2.2 Wind Turbine Modeling

The wind turbine is mainly composed by the rotor and the blades and it plays an important role in wind energy conversion. It is responsible by extracting power from the wind and passing it on to the electric generator shaft (SLOOTWEG and KLING, 2003).

It is well known that the wind kinetic energy (J/m^3) is given by Equation (10).

$$E = \frac{1}{2} m v_{wind}^2 \tag{10}$$

Where:

v_{wind}: wind speed (m/s); ω

m: mass of air (kg).

This equation can be represented in the form of wind power P_{wind} (*Watts*) by Equation (11).

$$P_{wind} = \frac{1}{2} \rho A v_{wind}^3 \tag{11}$$

Where:

A: área swept by turbine blades (m^2);

ρ: air density (ρ = 1.225 for standard pressure at sea level and 25 ºC) (kg/m^3).

Not all the power provided by wind can be used by the turbine. For this reason, it is expressed in Equation (12) the power coefficient or performance coefficient C_p, which is the ratio between the mechanical power available in the turbine shaft P_{mec} and the wind power P_{wind}.

$$C_p = \frac{P_{mec}}{P_{wind}} \tag{12}$$

From Equations (11) and (12), the mechanical power extracted from wind and used by turbine is obtained by Equation (13).

$$P_{mec} = \frac{1}{2} C_p(\lambda, \beta) \rho A v_{wind}^3 \tag{13}$$

Where:

λ: tip speed ratio (dimensionless);

β: blade pitch angle (degrees).

Tip speed ratio λ is defined by Equation (14):

$$\lambda = \frac{v_{blade}}{v_{wind}} = \frac{\omega_R R}{v_{wind}} \tag{14}$$

Where:

v_{blade}: turbine blade tip speed (m/s);

R: rotor radius (m);

ωR: rotor angular speed (rad/s).

In Figure 3 is illustrated the block diagram of pitch angle control, which is intended to limit the mechanical power transferred to the PMSG. Thus, it ensures that wind turbine power is kept close to its rated value for very high wind speeds (HEIER, 1998).

Figure 3 – Pitch angle control block diagram

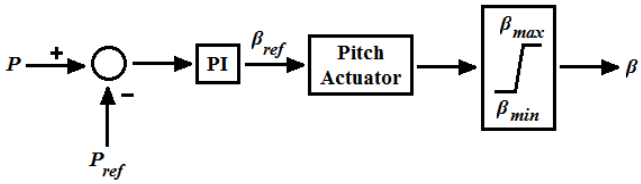

Again, as the adopted wind turbine model is not available in ATPDraw libraries, it was necessary to develop it using the MODELS interface. Thus, a new block component representing the wind turbine was also constructed, as illustrated in Figure 4, with three inputs nodes (wind speed, mechanical speed and electromagnetic torque) and one output node (accelerating torque).

Figure 4 – Wind turbine block

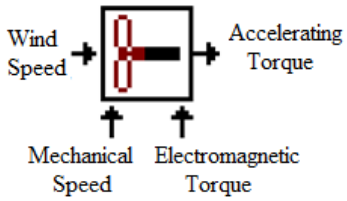

2.2 PMSG Modeling

This work employs a synchronous generator with a high number of poles because of low rotational speeds derived from its direct connection to the wind turbine shaft. The machine comprises 3-phase armature windings at stator and a permanent magnet field at rotor to ensure a constant magnetic flux. This last feature avoids the need of a DC excitation source.

An arrangement of the PMSG with only two poles is shown in Figure 5, where *aa*', *bb*', *cc*' represent the armature windings placed at machine stator.

Figure 5 – PMSG physical topology

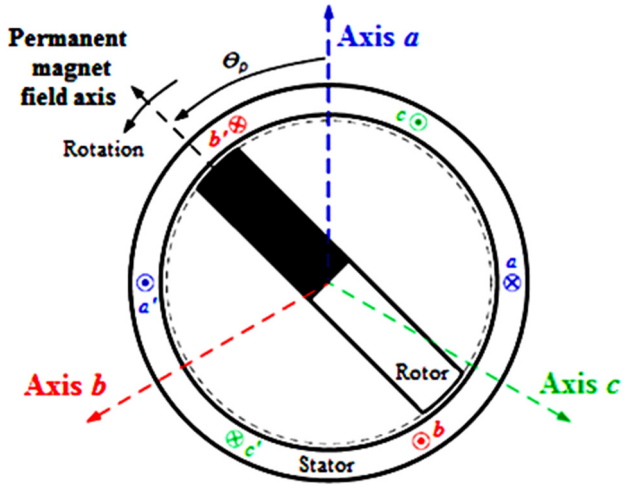

The PMSG model is based on linkage flux expressions of conventional synchronous machine (ANDERSON and FOUAD, 1977; KUNDUR, 1994) employing modeling techniques in ABC reference frame. It is important to point that some adjustments were performed in order to consider the flux produced by the rotor permanent magnet. This strategy modified the conventional synchronous machine equations where rotor magnetic field is produced by DC exciters.

The equations that relate voltages, currents and magnetic fluxes of the PMSG adopted here are:

$$[V] = -[R_S]\cdot[I] - \frac{\partial[\lambda_S]}{\partial t} \tag{15}$$

$$[\lambda_S] = \begin{bmatrix}\lambda_a\\ \lambda_b\\ \lambda_c\end{bmatrix} = \begin{bmatrix} L_{aa} & L_{ab} & L_{ac} & k_{af}\\ L_{ba} & L_{bb} & L_{bc} & k_{bf}\\ L_{ca} & L_{cb} & L_{cc} & k_{cf}\end{bmatrix}\cdot\begin{bmatrix} i_a\\ i_b\\ i_c\\ F_{PM}\end{bmatrix} \tag{16}$$

Where:

(V), (I) and (λ_S): vectors of voltages, currents and linkage fluxes of a, b, c phases;

(RS): diagonal matrix of winding resistances of a, b, c phases;

λa, λb and λc: linkage fluxes of a, b, c phases;

ia, ib and ic: currents of a, b, c phases;

FPM: magnetic flux of rotor permanent magnet.

The other elements required in the PMSG formulation are:

- Stator self-inductances (i = a, b or c):

$$L_{ii} = -L_S + L_m\cos[2(\theta_e + \alpha_{ii})] \tag{17}$$

- Stator mutual inductances (i or j = a, b or c and $i \neq j$):

$$L_{ij} = -M_S + L_m\cos[2(\theta_e + \alpha_{ii})] \tag{18}$$

- Coupling factor between the constant rotor field and stator armature windings considering the rotor position:

$$k_{iF} = F_{coup}\cos(\theta_e + \alpha_{iF}) \tag{19}$$

Where:

θ_e: electrical angle between the phase-a axis and the rotor field axis;

L_S e M_S: constant components of stator self and mutual inductances;

L_m: variable components of stator self and mutual inductances;

F_{coup}: coupling factor between the rotor field and stator armature windings (from 0 to1).

Note: angles α_{ij} are determined according to the relative position between the stator windings (a, b, c) and rotor field (F), as presented in Table 1 below.

Table 1 – a_{ij} Angles values

α_{ij}		j			
		a	**b**	**c**	**F**
i	**a**	0	π/6	5π/6	0
	b	π/6	-2π/3	-π/2	-2π/3
	c	5π/6	-π/2	2π/3	2π/3

The values R_S, L_S, M_S and L_m for the stator windings are calculated from generator data supplied by the manufacturer through Equations (20) to (27).

$$R_S = R_{S\_pu}\frac{V_B^2}{S_B} \tag{20}$$

$$L_S = L_{S\_pu}L_B \tag{21}$$

$$L_{S\_pu} = \frac{1}{3}(X_d + X_q) \tag{22}$$

$$L_B = \frac{V_B/S_B}{2\pi f_B} \tag{23}$$

$$M_S = M_{S\_pu}L_B \tag{24}$$

$$M_{S\_pu} = \frac{1}{6}(X_d + X_q) \tag{25}$$

$$L_m = L_{m\_pu}L_B \tag{26}$$

$$L_{m\_pu} = \frac{1}{3}(X_d - X_q) \tag{27}$$

Where:

R_S: phase winding resistance (ohms);

RS_pu: per-unit value of resistance (pu);

VB: rated phase-to-phase voltage (V);

SB: rated three-phase power (VA);

LS: first coefficient of self-inductances (H);

LS_pu: per-unit value of inductance (pu);

LB: base inductance (H);

Xd: per-unit direct axis reactance (pu);

Xq: per-unit quadrature axis reactance (pu);

Xl: per-unit leakage reactance (pu);

fB: rated frequency (Hz);

MS: first coefficient of mutual inductances (H);

Lm: second coefficient of self and mutual inductances (H).

The electromagnetic torque T_{elet} produced by PMSG is defined by Equation (28):

$$T_{elet} = \frac{n_p}{2} F_{PM} \sum_i i_i \frac{\partial L_{iF}}{\partial \theta_e} \quad (28)$$

Where:

n_p: number of poles.

Equation (29) gives the PMSG swing expression.

$$T_a = T_{mec} - T_{elet} = J \frac{\partial \omega}{\partial t} \quad (29)$$

Where:

T_{mec}: mechanical torque (N.m);

ω: rotor mechanical speed (rad/s);

J: turbine inertia moment.

As ATPDraw libraries do not include the above-mentioned PMSG model, once more it was necessary to create it by the MODELS interface. Thus, a new block component representing the PMSG was also built, as shown in Figure 6, and connected to the wind turbine block.

Figure 6 – PMSG block

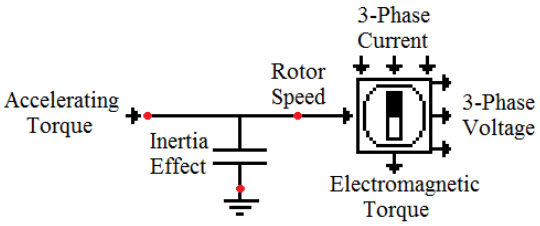

Notice that the mechanical rotor speed is extracted by the voltage applied on the capacitor, whose capacitance represents the inertia of the turbine-generator set. It was used the electromechanical analogy between equation (29) ($T_a = J\,\partial\omega/\partial t$) and the differential equation that represents the capacitor loading ($i_c = C\,\partial v/\partial t$). Besides, the PMSG icon contains input nodes for rotor speed and *a, b, c* armature phase currents, while the output nodes are electromagnetic torque and *a, b, c* terminal phase voltages.

2.3 AC-DC Uncontrolled Rectifier and DC Link Models

The full-wave rectifier and the DC link are represented by a 6-pulse 3-phase diode bridge, a smoothing inductor *L* and an output capacitor *C*, as shown in Figure 7.

Figure 7 – Full-wave rectifier and the DC link topology

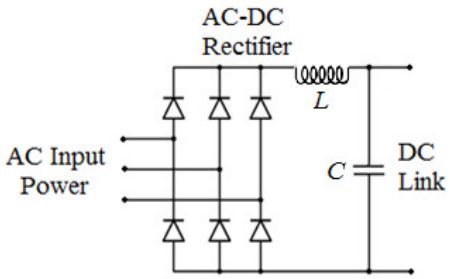

Further details about these devices are not presented since all their components are readily available in ATPDraw libraries and widespread in the related literature.

2.4 Frequency Inverter Modeling

The 3-phase frequency inverter considered in this work comprises six controlled thyristors, as illustrated in Figure 8, and produces an AC voltage system, from DC link voltage, which is connected to the isolated load. As this device represents an important unit for the integration of wind farms to both power grid and isolated loads, its control system must be configured so as to obtain an appropriate interconnection in steady-state or dynamical condition ω.

Figure 8 – Frequency inverter topology

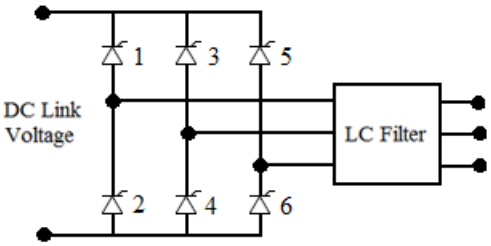

In this work, the classical vector control strategy is used for the definition of the firing logic requirements for the six thyristors (SCHAUDER and MEHTA, 1993). Besides, using the PWM technique, also widely applied in this study field, the 6-thyristor firing sequence is achieved, thereby determining the characteristics of the 3-phase voltage produced at the inverter output terminals (ABDELKAFI and KRICHEN, 2011).

In Figure 9 is depicted the block diagram of load voltage magnitude control performed by frequency inverter, which allows the maintenance of load voltage levels within appropriate ranges even under wind speed variations and sudden load changes. From monitoring the isolated load voltage, the control system defines the variation of the inverter modulation factor (m_p), which will act to increase/decrease the AC voltage produced at its terminals.

Figure 9 – Block diagram of load voltage magnitude control

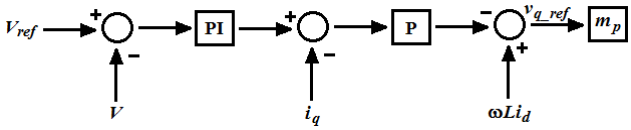

The inverter modulation factor is calculated according to Equation 30. It is also important to mention that, at the output terminals of the frequency inverter, an LC filter is connected, whose role is to filter the voltage wave obtained, bringing it much closer to sinusoidal shape.

$$m_p = \frac{1}{v_{q\_ref}} \tag{30}$$

The required components (thyristors, resistors and capacitors) for the construction of frequency inverter electric circuit are readily available in ATPDraw libraries. However, the development of two new blocks by MODELS interface is necessary, as shown in Figure 10.

The first one takes into account the load voltage magnitude control strategy, with eight input nodes (positive and negative DC link voltages, *a, b, c* armature phase currents and *a, b, c* terminal phase voltages) and one single output node (modulation factor), which is also taken to the input node of the second icon. This block provides six output nodes representing the 6-thyristor firing.

Figure 10 – Frequency inverter blocks

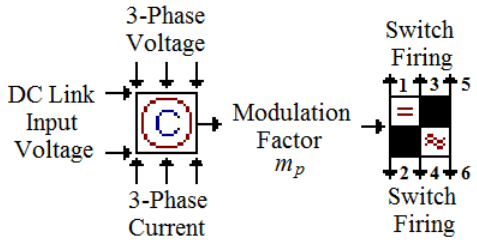

2.5 Transformer Model

The transformer works to raise the frequency inverter output voltage to a suitable value demanded by isolated loads. In addition, when wind farms are connected to large power grids, the transformer increases this voltage value to comply with power transmission common ranges.

This work employs a 2-winding transformer, whose model is readily available in ATPDraw libraries, including the nonlinear feature of core ferromagnetic material, but such effect was disregarded since it is not a major influence on the objectives sought here. Further details about this device are not presented because transformer modeling and operation are widespread in the literature.

2.6 Isolated Load Model

As mentioned, the WECS modeled in this work supplies a 3-phase isolated load, which is characterized as having an inductive power factor of 0.92. This value is chosen so as to represent a real industrial load connected to a distribution power system. The load components (resistors and inductors) are readily available in ATPDraw libraries, not requiring further information about their models.

3 – COMPUTER STUDIES

This section aims to present the computer studies performed to verify the functionality of the mathematical models presented for the WECS and to evaluate the load voltage magnitude control developed. For that, simulations were performed using the software ATP, considering the overall electric system under distinct operating conditions.

The parameters of wind turbine and PMSG models, used in this work, are listed in Tables 2 and 3, respectively.

Table 2 – Wind turbine parameters

Wind turbine rated power (MW)	2
Rotor diameter (m)	62
Rated wind speed (m/s)	13.52
Turbine inertia moment (kg·m^2)	2.92×10^6

Table 3 – PMSG parameters

PMSG rated power (MW)	2
PMSG rated voltage (kV)	0.69
PMSG rated frequency (Hz)	13
PMSG number of poles	64
Stator winding resistance (p.u.)	0.042
Direct axis reactance (p.u.)	1.05
Quadrature axis reactance (p.u.)	0.75
Magnetic flux of rotor PM (Wb)	7

3.1 Wind Disturbances

In Figure 11 is illustrated the wind behavior considered for computer simulations. Initially, the wind speed was set at its optimal value of 13.52 m/s. During the time period from t = 10 s to t = 20 s, a positive wind gust with maximum speed rise of 4 m/s was applied. Later, at t = 35 s, a negative wind ramp was started, which reached a maximum speed drop of 2 m/s at t = 43 s.

Figure 11 – Wind speed behavior

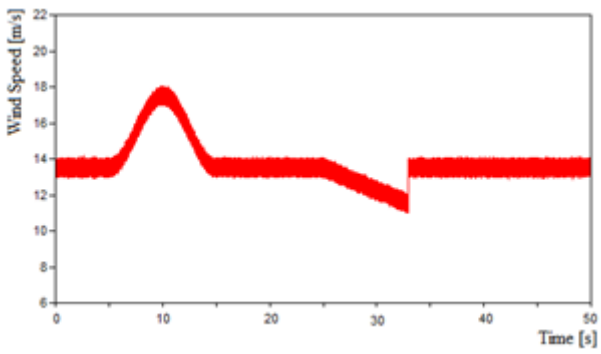

In Figure 12 is depicted the mechanical speed of the wind turbine rotor, while in Figure 13 is shown the corresponding terminal voltage frequency produced by

PMSG. The solid lines indicate that prior to the occurrence of the wind disturbances, i.e., in steady state condition, the angular speed of the rotor was 3.7 rad/s, corresponding to the electric frequency of 18.7 Hz. Although the PMSG rated electric frequency was 13.0 Hz, a larger electric frequency was obtained since that the load supplied by the wind generator was below its rated value.

The occurrence of the positive wind gust caused the operation of the pitch control, which achieved a maximum angle of approximately 18.0, as illustrated in Figure 14, following the wind behavior. This fact resulted in attenuation of both mechanical speed and PMSG voltage frequency rises, which started at t = 10 s in Figures 12 and 13, respectively. The dotted curves illustrate that such variables would have an increase of approximately 22% if the pitch control were turned off.

During the presence of negative wind ramp, there was a reduction of rotor speed and voltage frequency supplied by PMSG, which reached minimum values of 3.41 rad/s and 17.4 Hz, respectively, as seen in Figures 12 and 13.

Figure 12 – Mechanical speed behavior

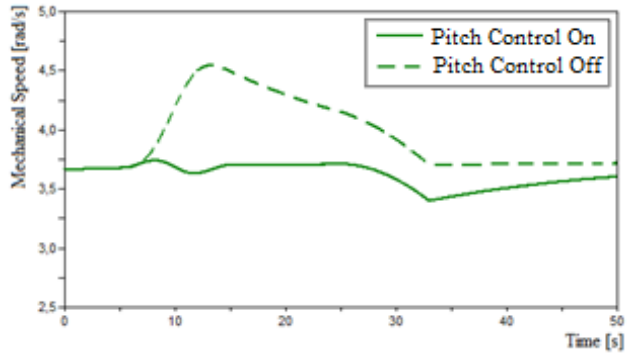

Figure 13 – PMSG terminal voltage frequency behavior

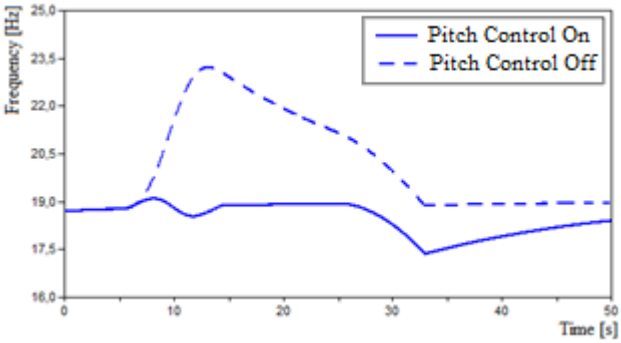

Figure 14 – Pitch control behavior

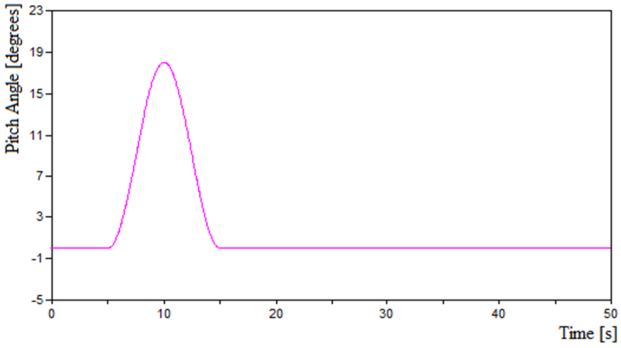

Figure 15 shows that the DC link voltage in steady state condition was 1420 V, approximately. The wind gust caused the operation of the pitch control, which allowed the maintenance of DC voltage close to the steady state value. However, the negative wind ramp caused a DC voltage decline to about 1350 V. The dotted line illustrates the DC link voltage behavior if the pitch control were turned off, achieving a maximum value close to 1720 V.

Figure 15 – DC link voltage behavior

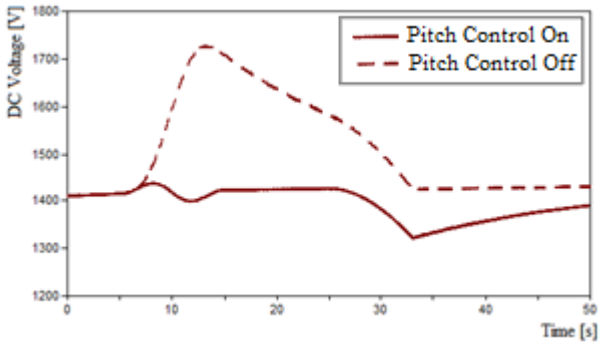

The dotted curve from Figure 16 illustrates the isolated load voltage when both frequency inverter and pitch controls were turned off. In steady state condition, the load voltage was 13.8 kV and, during the positive wind gust, it achieved 16.2 kV, whereas at the end of the negative wind ramp it dropped to 13.4 kV. The solid line indicates that the load voltage could be maintained at 13.8 kV if both frequency inverter and pitch controls were enabled.

Figure 16 – Isolated load voltage behavior

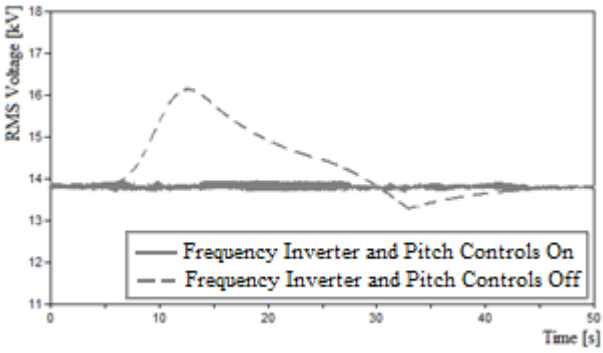

3.2 Sudden Load Changes

This section shows the voltage behavior for distinct sudden load changes taking into account a constant base wind speed of 13.52 m/s with the noise component. It is important to mention that other WECS variables, such as turbine mechanical speed and PMSG voltage frequency, will have similar variations and, therefore, they need not to be presented here. Initially, the load was 1.587 MVA, with approximately 0.92 power factor. At t = 10 s there was 20% load shedding, which decreased the power value to about 1.270 MVA. Later, at t = 35 s, this load was increased by 30%, raising the power value to 1.650 MVA.

The dotted curve from Figure 17 illustrates the isolated load voltage for both frequency inverter and pitch controls switched off. In steady state condition, the load voltage was 13.8 kV and, after the load shedding, it increased to a value near to 16.5 kV. On the other hand, after the load increase, the voltage decreased to a value close to 13.2 kV. The solid line indicates that the load voltage could be maintained at 13.8 kV if both frequency inverter and pitch controls were switched on.

Figure 17 – Isolated load voltage behavior

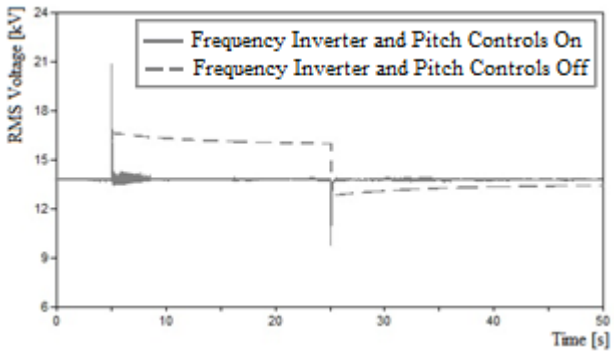

CONCLUSIONS

This paper presented the mathematical and computational modeling in ABC reference frame of a Wind Energy Conversion System (WECS) equipped with a Permanent Magnet Synchronous Generator (PMSG), supplying an isolated load with 0.92 power factor. The objective of this work was to present the overall modeling developed for the WECS and to analyze the operation of pitch and frequency inverter controls to face sudden changes in wind or load.

Firstly, changes in base wind speed were simulated to represent a positive gust and a negative ramp. In both cases the operation of the frequency inverter control ensured the isolated load voltage to be kept in its rated value. The occurrence of positive wind gust also caused the pitch control operation and, consequently, maximum values for mechanical speed and turbine power could be achieved. However, such action was not performed during the negative wind ramp as expected since the maximum power limit was not exceeded.

Therefore, it was shown that the rated (maximum) WECS operation condition was tracked by the pitch control under the event of wind speed increase. It was also pointed out that the absence of such control could cause a large rise in both rotor speed and PMSG voltage frequency, which would eventually provoke electrical and mechanical damages in the wind turbine-generator set.

Secondly, distinct sudden load changes were simulated during a constant base wind speed scenario. It was noted that, when both pitch and frequency inverter controls were turned off, the partial load shedding would cause an elevation of the isolated load voltage, while a load increase would lead to a voltage rise. However, when the pitch and frequency inverter control were enabled, the load voltage could be kept close to the rated value (13.8 kV).

The developed mathematical modeling of the PMSG-based wind turbine in ABC system has shown to be a feasible technique for dynamic analysis of wind generators. Besides, the operation of the pitch and frequency inverter controls was able to maintain an appropriate voltage level for the isolated load.

The behavior of the main parameters related to the WECS performance (rotor speed, PMSG voltage frequency, pitch control angle, load voltage) in face of significant variations of wind speed (gust and ramp) or load power confirmed the efficiency of the developed modeling. Therefore, the free software Alternative Transients Program (ATP), especially through its MODELS interface, allowed the development of adequate representations for all WECS components.

REFERENCES

ABDELKAFI, A.; KRICHEN, L. New Strategy of Pitch Angle Control for Energy Management of a Wind Farm. **Energy**, v. 36, p. 1470-1479, March, 2011. http://dx.doi.org/10.1016/j.energy.2011.01.021.

ALEPUZ, S.; CALLE, A.; BUSQUETS-MONGE, S.; KOURO, S.; BIN, W. Use of Stored Energy in PMSG Rotor Inertia for Low-Voltage Ride Through in Back-to-Back NPC Converter-Based Wind Power Systems. **IEEE Transactions on Industrial Electronics**, v. 6, n. 5, p. 1787-1796, May, 2013. http://dx.doi.org/10.1109/TIE.2012.2190954.

ANDERSON, P. M.; BOSE, A. Stability Simulation of Wind Turbine System. **IEEE Transactions on Power Apparatus and Systems**, v. PAS-102, n. 12, p. 3791-3795, 1983. http://dx.doi.org/10.1109/TPAS.1983.317873.

ANDERSON, P. M.; FOUAD, A. A. **Power System Control and Stability**. The Iowa State University Press, USA, 1977.

BARAZARTE, R.; GONZÁLEZ, G; HALL, E. Comparison of Electric Generators used for Wind Generation. **IEEE Latin America Transactions**, v. 9, n. 7, December, 2011. http://dx.doi.org/10.1109/TLA.2011.6129700.

BRAY, J.; FAIR, R; HARAN, K. Wind and Ocean Power Generators. **IEEE Transactions on Applied Superconductivity**, v. 24, n. 3, September, 2013.

BYSTRYK, J.; SULLIVANN, P. E. Small Wind Turbine Control in Intermittent Wind Gusts. **Journal of Wind Engineering & Industrial Aerodynamics**, v. 99, n. 5, p. 624-637, May, 2011. http://dx.doi.org/10.1016/j.jweia.2011.03.001.

KUNDUR, P. **Power System Stability and Control**. McGraw-Hill, Inc, 1994.

FREIRE, N., CARDOSO, A. J. M. A Fault-Tolerant Direct Controlled PMSG Drive for Wind Energy Conversion Systems. **IEEE Transactions on Industrial Electronics**, v. 61, n. 2, February, 2014. http://dx.doi.org/10.1109/TIE.2013.2251734.

HEIER, S. **Grid Integration of Wind Energy Conversion System**. John Wiley & Sons, England, 1998.

LI, P.; TANG, J.; ZHANG, L.; LIAN, C. Independent Control of Active and Reactive Power of the Grid-Connected Inverter. **International Conference on Electrical Machines and Systems**, October, 2008.

LÓPEZ-ORTIZ, E. N.; CAMPOS-GAONA D.; MORENO-GOYTIA, E. L. Modelling of a Wind Turbine with Permanent Magnet Synchronous Generator. **North American Power Symposium** (NAPS), September, 2012.

SCHAUDER, C.; MEHTA, H. Vector Analysis and Control of Advanced Static Var Compensators. **IEEE Proceedings-C**, v. 40, n. 4, p. 299 – 306, July, 1993.

SHARIATPANAH, H.; FADAEINEDJAD, R.; RASHIDINEJAD, M. A New Model for PMSG-Based Wind Turbine With Yaw Control. **IEEE Transactions on Energy Conversion**, v. 28, n. 4, December, 2013. http://dx.doi.org/10.1109/TEC.2013.2281814.

SLOOTWEG, J. G.; KLING, W. L. The Impact of Large Scale Wind Power Generation on Power System Oscillations. **Electric Power Systems Research**, v. 67, p. 9-20, 2003. http://dx.doi.org/10.1016/S0378-7796(03)00089-0.

BIOGRAPHY

Daniel Araújo Caixeta was born in Uberlândia, MG, Brazil, in 1985. He was graduated in Electrical Engineering in Federal University of Uberlândia in 2008. He obtained the master degree in Electrical Engineering from Federal University of Santa Catarina in 2010. Presently he is a doctorate student in Postgraduate Program of Electrical Engineering in Federal University of Uberlândia. He works at Power System Dynamics Laboratory. His research areas are: Wind Energy, Distributed Generation, Transient and Voltage Stability, Smart Grids and Data Mining Applied to Power Systems.

Geraldo Caixeta Guimarães was graduated in Electrical Engineering in Federal University of Uberlândia in 1977. He obtained the master degree in Electrical Engineering from Federal University of Santa Catarina in 1984 and Ph.D. degree in Electrical Engineering from University of Aberdeen, Aberdeen, United Kingdom, in 1990. Presently he is professor at Electrical Engineering Department of Federal University of Uberlândia. His research areas are: Wind Energy, Distributed Generation, Dynamic and Control of Power Systems, Power Flow, Transient and Voltage Stability, Applied Electromagnetics.

Marcelo Lynce Ribeiro Chaves was born in Ituiutaba, MG, Brazil, in 1951. He was graduated in Electrical Engineering in 1975 and obtained the master degree in Electrical Engineering in 1985, both from Federal University of Uberlândia. He finished the doctorate course in 1995 in Unicamp, Campinas, Brazil. At present he is professor in Federal University of Uberlândia. His areas of interest are: Electric Drives, Electromagnetic Transients and Transformers Modeling and Power System Analysis.